

Article

Brazil Wave Climate from a High-Resolution Wave Hindcast

Camila de Sa Cotrim ¹ , Alvaro Semedo ^{2,3,*} and Gil Lemos ³

¹ Environmental Hydraulics Institute “IH Cantabria”, Universidad de Cantabria, 39011 Santander, Spain; camila.desacotrim@unican.es

² IHE Delft, Department of Coastal, Urban Risk and Resilience, Westvest 7, 2611 Delft, The Netherlands

³ Instituto Dom Luiz (IDL), Faculdade de Ciências, Universidade de Lisboa, Campo Grande, 1749-016 Lisbon, Portugal; grlemos@fc.ul.pt

* Correspondence: a.semedo@un-ihe.org

Abstract: A detailed climatology of ocean wind waves in the South Atlantic Ocean, based on ERA-5 reanalysis and in a higher-resolution wave hindcast (ERA-5H), both developed by the European Centre for Medium-Range Weather Forecasts, is presented. The higher resolution of the wave fields in the ERA-5H (22 km) allowed for a better description of the wind sea and swell features compared to previous global and regional studies along the Brazilian coast. Overall, it is shown that swell waves are more prevalent and carry more energy in the offshore area of the study area, while wind sea waves dominate the nearshore regions, especially along the northern coast of Brazil. The influence of different climate indices on the significant wave heights patterns is also presented, with two behavioral groups showing opposite correlations to the North Atlantic Oscillation and Southern Annular Mode than to the Southern Oscillation Index. The analysis of the decadal trends of wind sea and swell heights during the ERA-5H period (1979–2020) shows that the long-term trends of the total significant wave height in the South Atlantic Ocean are mostly due to swell events and the wave propagation effect from Southern Ocean storms.

Keywords: wave analysis; ERA5; South Atlantic Ocean



Citation: Cotrim, C.S.; Semedo, A.; Lemos, G. Brazil Wave Climate from a High-Resolution Wave Hindcast. *Climate* **2022**, *10*, 53. <https://doi.org/10.3390/cli10040053>

Academic Editor: Steven McNulty

Received: 26 February 2022

Accepted: 29 March 2022

Published: 31 March 2022

Publisher’s Note: MDPI stays neutral with regard to jurisdictional claims in published maps and institutional affiliations.



Copyright: © 2022 by the authors. Licensee MDPI, Basel, Switzerland. This article is an open access article distributed under the terms and conditions of the Creative Commons Attribution (CC BY) license (<https://creativecommons.org/licenses/by/4.0/>).

1. Introduction

Waves result from the transfer of energy from the atmosphere to the ocean through the wind, therefore being closely related to variations in atmospheric regimes, which have higher temporal and spatial variability [1,2]. Two types of waves can be observed on the ocean’s surface: Wind sea and swell [3–5]. On the one hand, wind seas are short-period waves, generated by the overlaying winds, with a wave phase speed lower than the local wind speed. On the other hand, swells are long-period waves, generated afar, to a distance that can be thousands of kilometers away, with a wave phase speed that exceeds the local wind speed. Thus, when analyzing the wave climate, it is useful to divide the wave data into both wind sea climate and swell climate analyses [4,6,7], and any relationship with local winds must be established with caution.

Besides the wind sea and swell separation, waves are also analyzed regarding different wave parameters. These can be computed from the ocean wave spectrum, given that waves on the ocean surface can be interpreted as the sum of regular wave components with random phase angles and different frequencies. One of the most commonly used wave parameters is the significant wave height (H_s), defined as the average height of the highest one-third of all the waves if computed from a wave record. Otherwise, when computed from wave spectra, $H_s = 4\sqrt{m_0}$, where m_0 is the zeroth spectral moment, computed as $m_0 = \int_0^\infty \int_0^\infty f^0 E(\theta, f)$, where $E(\theta, f)$ is the two-dimensional (2D) wave (variance) spectrum, and θ and f are the direction and the frequency, respectively. The 2D wave variance spectrum is related to the total energy content of the sea state [8]. The mean wave period (T_m) can also be calculated from the wave spectrum, as well as the mean wave direction

(θ_m). Additionally, H_s , T_m , and θ_m can also be computed separately for the wind sea and swell components of the sea state via partitioning of the wave spectrum, thus obtaining the wind sea and swell significant wave heights (H_s^w and H_s^s , respectively), mean wave periods (T_m^w and T_m^s), and mean directions (θ_m^w and θ_m^s). Consider [4,7,9] for further details.

Since the wave climate is dominated by local and remote atmospheric conditions, it can also be analyzed regarding its temporal, directional, and spectral characteristics. These include the variability and periodicity of wave parameters and their association with climate indices [10]. Waves represent a key process within the climate system and can influence not only energy transfers between the ocean and the atmosphere but also heat and mass [11]. Thus, understanding the wave climate is important, for example, for monitoring of coastal erosion and sediment transport, coastal and offshore engineering, ship routing, environmental studies, and wave energy estimation for renewable energy purposes [12].

Given the potential impacts on coastal morphology and beach dynamics, extreme waves deserve special attention as part of the wave climate of a region, particularly in land-falling storms. Extreme wave events are responsible for the most drastic changes in coastal morphological evolution [13], frequently leading to extreme erosion processes. Moreover, understanding the patterns behind extreme waves is important for any coastal management and engineering activities, not to mention coastal hazard studies. These extreme wave heights are usually associated with storms, sometimes taking place far away [14]. Additionally, storm waves are often combined with storm surges, leading to severe effects in coastal zones [15]. For that matter, the assessment of the present wave climate is crucial to determine potential changes and trends, due to natural climate fluctuations, or anthropogenically induced climate change processes [4,16–19].

The most direct and obvious approach to studying wave climate is through observations. In situ wave measurements performed with oceanographic buoys represent the most realistic data, but they are local observations, geographically sparse, and limited [20,21]. On the other hand, even though remote sensing provides global coverage through satellite altimetry, it also represents a short time series (about 25 years) and low temporal and spatial resolution [22]. Therefore, numerical models are more often used and commonly applied to conduct wave climate studies, using reanalysis and hindcast data, where recent past wave events are simulated considering historical wind data in order to understand present wave climate [10]. The European Centre for Medium-Range Weather Forecasts (ECMWF) has a long tradition of producing reanalysis data. The ECMWF started atmospheric reanalysis in 1979 with the start of the satellite era. Up until the release of ERA-20C, ERA-Interim was the most complete ECMWF product. The evolution of forecast and hindcast methods eventually led to the development of ERA-5, which is the main dataset used in the present study.

A reanalysis relies on interpreting, relating, and combining different observations from multiple sources that document the evolution of the global atmosphere, ocean (including waves), land surface, cryosphere, and the carbon cycle. Equations of motion and physical processes are used to generate data products based on the assimilated information, which combine the first model result (short-range forecast) with observations (in the “analysis” step; [23]). The temporal consistency of the reanalysis depends on the quality of the input observations. These tools play an important role in improving observation systems through the feedback loop, which results from advances in data assimilation and the development of better forecast models. The improvement of forecasting systems is largely due to the evolution of observation systems over the last three decades, which is mainly a result of the advances in satellite technology [24,25].

Global wave climate studies including the South Atlantic Ocean (SAO) have been recently performed [4,11,26]. However, most wave climate studies are focused on the North Atlantic Ocean (NATL) [16,27–29]. Wave climate studies in the SAO are relatively limited, mostly regional, and lack long-term assessments (of more than 30 years). For instance, in Brazil, [30] studied the coast of Ceará in the north, and [31,32] analyzed the waves along the

southern region in Santa Catarina and Rio Grande do Sul, respectively. The longest analyses in Brazil were performed by [33,34] in the southern region of the country, and by [35] in the southeast. Other authors, including [36,37], exemplify the few studies covering the entire Brazilian coast, based on reanalysis data. However, only the latter truly represents long-term analysis.

Considering the extension of the Brazilian coast, its wave climate is determined by winds originating in the SAO and the Southern Ocean, involving three large atmospheric systems: The SAO (including the respective Southern Ocean sector) extratropical storm belt, the Intertropical Convergence Zone (ITCZ), and the respective trade winds, from both hemispheres. Given these major mechanisms responsible for wave generation in the SAO, it can be concluded that the Brazilian coastline is influenced by two main wave systems: East-northeastern waves and south-southeastern waves [38]. The relevance of these atmospheric and wave systems across the coast of Brazil varies with the latitude and coastal orientation. Moreover, along the section between the southernmost region to the eastern region of the Brazilian coast, the austral winter months are the most energetic ones, whilst the most energetic period in the north region is from December to March, indicating different seasonality patterns along the study area.

The present study details, for the first time, the present wave climate across the entire coast of Brazil using wave data from an ECMWF high-resolution wave hindcast. This hindcast has been produced using ERA-5 reanalysis winds and sea ice concentration (SIC) and will henceforth be designated as ERA-5H. The goal of this study is to examine the wave climate variability and long-term trends along the coast of Brazil, based on the high-resolution ERA-5H hindcast, from 1979 to 2020.

The outline of this paper is as follows: Section 2 details the ERA-5 reanalysis and ERA-5H hindcast data, as well as in situ datasets, and a summary of the methodology used. The results and description of the wave climate off the coast of Brazil are presented in Section 3. Section 4 presents the key point analysis in which a comparison with in situ data was performed. Lastly, a summary of the study and concluding remarks are presented in Section 5.

2. Materials and Methods

2.1. The ECMWF ERA-5 Based Wave Hindcast

Reanalysis data are used for climate studies when there is a lack of observations. Due to the hectic nature of the atmosphere, models need constant updates in order to perform corrections to their results. Reanalyses use data assimilation to correct them by mixing observations and model simulations. On the other hand, the hindcast approach is based on running atmospheric and wave models for a historical period, but without data assimilation.

Produced with the purpose of replacing ERA-Interim, the ERA-5 reanalysis provides a comprehensive high-resolution record of the global atmosphere, land surface, and ocean wind waves from 1950 onwards. Meanwhile, ERA-5H is a long global wave model stand-alone run (i.e., not coupled) forced by ERA-5 hourly 10 m neutral winds, surface air density, gustiness, and SIC. Because no wave data assimilation was used with this hindcast, it can also be seen as a benchmark of the quality of ERA-5 atmospheric forcing.

Even though the outputs of both ERA-5 and ERA-5H are hourly, their horizontal resolution is very different, with the latter showing a higher resolution [39]. The horizontal resolution of ERA-5 is 31 km for the atmosphere and 40 km for the waves, while the ERA-5H wave resolution is 0.2° (22 km). Their spectral resolutions are also different, with ERA-5 showing 24 directions and 30 logarithmically spaced frequencies, while ERA-5H presents 36 directions and 36 frequencies. Moreover, ERA-5H uses a more recent global bathymetry, as presented in Table 1. Furthermore, ERA-5H was produced with ERA-5 winds and a modified version of the WAM wave model.

Table 1. Comparison between ERA-5 and ERA-5H information [39].

Parameter	ERA-5	ERA-5H
Period covered	1950–present	1979–present
Data product	Reanalysis	Hindcast
Temporal resolution	1 h	1 h
Spatial resolution (waves)	40 km	22 km
Spectral resolution	24 directions, 30 logarithmically spaced frequencies	36 directions and 36 frequencies
Bathymetry	ETOPO2	ETOPO1
Assimilation scheme	4D-Var	-
IFS ¹ model cycle	41r2 (2016)	46r1 (2019)

¹ IFS = Integrated Forecasting System.

To better exemplify the differences between ERA-5 and ERA-5H, the spatial distributions of H_s and wave energy flux (P_w), as well as extreme wave conditions, in the study area are presented in the Supplementary Material. We should highlight the better performance of the ERA-5H, especially with the differences near the coast for extreme values of P_w along the eastern region of Brazil.

To determine the wave climate variability along the coast of Brazil, several wave parameters were analyzed from 1979 to 2020, such as H_s , T_m , and θ_m . However, when analyzing the entire Atlantic Ocean basin, wind speed (U_{10}) and wind direction (φ) were examined based on ERA-5 data, while H_s and θ_m were based on ERA-5H.

2.2. In Situ Wave Observations

The ERA-5H data were also compared against in situ wave observations. From all the buoy data available since 1979 along the coast of Brazil, 5 buoys from PNBOIA (Programa Nacional de Bóias) were selected. Table 2 presents the position of the buoys used in the evaluation and their respective ERA-5H grid points, which have similar coordinates. The ERA-5H grid points were chosen as the closest ERA-5H points to the actual location of the corresponding buoys they were intended to be compared to. The variables extracted from the buoys included H_s , T_m , and U_{10} .

Table 2. Buoy details and their respective ERA-5H key points.

Region	Buoy (PNBOIA)	ERA-5H Key Point	Depth (m)	Time Frame	Latitude	Longitude
North	Fortaleza	P1	200	18/11/2016–20/05/2018	03°12.82' S	038°25.95' W
Northeast	Recife	P2	200	21/09/2012–06/04/2016	08°09.22' S	034°33.57' W
Northeast	Porto Seguro	P3	200	06/07/2012–19/12/2016	16°00.05' S	037°56.42' W
Southeast	Santos	P4	200	12/04/2011–09/12/2018	25°26.37' S	045°02.17' W
South	Rio Grande	P5	200	29/04/2009–09/03/2019	31°33.74' S	049°50.24' W

2.3. Methods

In order to better understand swell events in the region under study, a swell-tracking algorithm [40–42] was applied. With this, it was possible not only to quantify the events at different points of the coast but also to determine where they are coming from in order to evaluate the contribution of different storm generation areas.

The relationship between large-scale atmospheric forcing and the climatological variability of H_s was studied through spatial correlation analysis, based on Pearson correlation, against the climate patterns most representative over the SAO. The patterns included the North Atlantic Oscillation (NAO), the El Niño Southern Oscillation (ENSO) represented by the Southern Oscillation Index (SOI), and the Southern Annular Mode (SAM).

The evaluation of how well ERA-5H represents the wave climate of Brazil was determined by comparing the ERA-5H hindcast (y) against in situ observations (x). This was performed with the construction of scatter plots, as well as the computation of statistic parameters as described below.

BIAS represents the deviation between two variables, which can be defined as the difference between the averages of the time series:

$$BIAS = \text{sum}(y - x) / \text{length}(x). \tag{1}$$

The Root Mean Square Error (RMSE) measures the difference between an estimated value and the true value:

$$RMSE = \sqrt{\frac{1}{N} \sum_{i=1}^N (x_i - y_i)^2}. \tag{2}$$

The linear regression slope, or symmetric slope (SS), describes how much one can expect Y to change as X increases. In an ideal situation, SS = 1.

$$SS = \frac{\bar{y}}{\bar{x}}. \tag{3}$$

The Pearson correlation coefficient (ρ) is the measurement of how the two variables are related to each other, with 1 (−1) indicating a perfect correlation (anticorrelation).

$$\rho = \sqrt{\frac{\sum_{i=1}^N (x_i - \bar{x})^2}{\sum_{i=1}^N (y_i - \bar{y})^2 + \sum_{i=1}^N (x_i - \bar{x})^2}}. \tag{4}$$

The scatter index (SI) is the measurement of the dispersion with regard to the line $x = y$ (ideal).

$$SI = \frac{RMSE}{\bar{x}} * 100. \tag{5}$$

Finally, the intra-annual variability of wave parameters was examined for the same 5 key points used in the in situ observation analysis through monthly averages. The same points were used in the long-term variability analysis, but rather with linear trends of H_s , H_s^w , and H_s^s .

A summary of the methodology applied is presented in Figure 1.

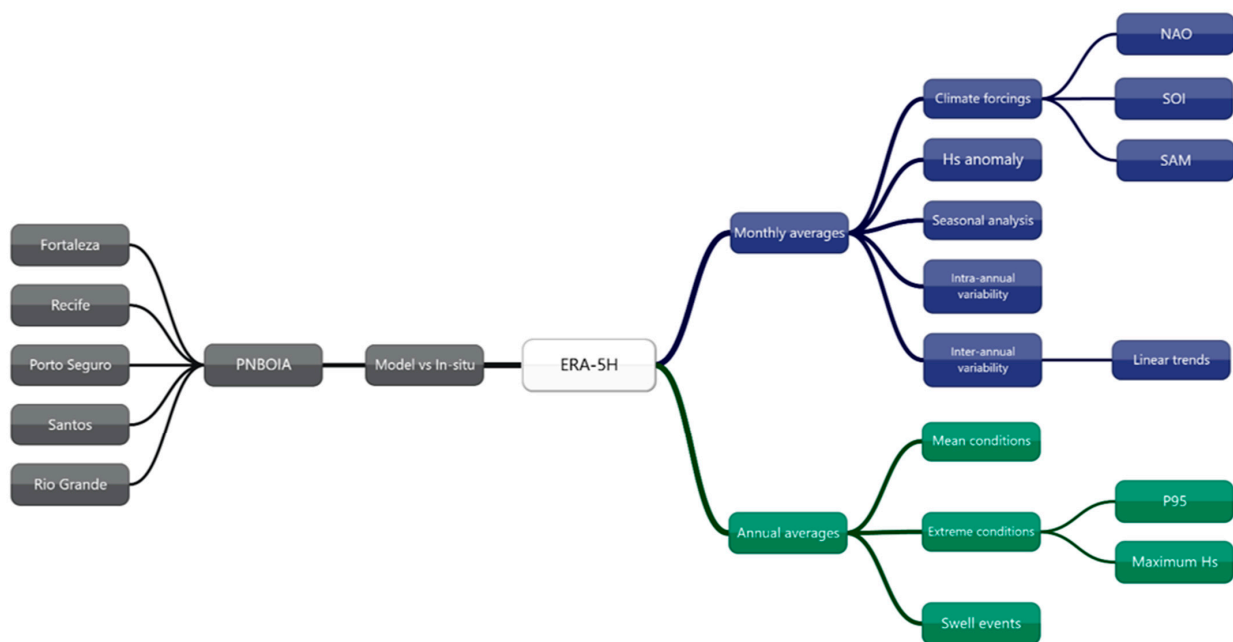


Figure 1. Flow chart of the summary of the methodology applied.

3. The Wave Climate of Brazil

3.1. Atlantic Ocean Wind and Wave Climates

The climatological annual means of U_{10} and φ , as well as H_s and θ_m , for the entire Atlantic Ocean, are shown in Figure 2 (ERA-5 reanalysis data). For both hemispheres, the extratropical regions present the highest values of U_{10} and H_s . In these regions, the yearly mean U_{10} can reach up to 12 m/s, while the mean H_s can be higher than 4 m. The lowest U_{10} values can be found approximately where the centers of the respective semi-permanent anticyclone systems are located in each hemisphere (the Azores and the St. Helena High, respectively), and along the western coast of the African continent. Regarding the mean H_s , the lowest values are found in the tropical and subtropical regions (the “swell pools”; [43]) as well as closer to the coasts. In fact, between the latitudes of 30° S and 30° N, the mean H_s is lower than 2 m.

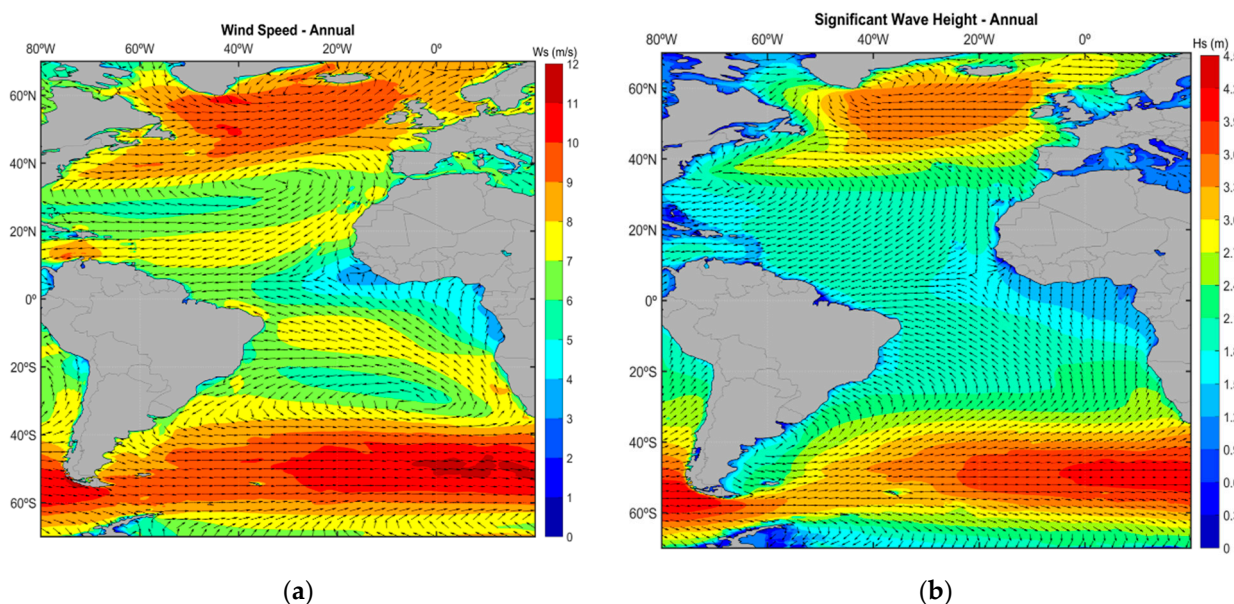


Figure 2. (a) Annual mean U_{10} ($\text{m}\cdot\text{s}^{-1}$) and φ ($^{\circ}$) for the Atlantic Ocean. (b) Annual mean H_s (m) and θ_m ($^{\circ}$) for the Atlantic Ocean.

3.2. Brazil's Mean Wave Heights and Directions (Wind Sea and Swell)

Figure 3 presents the climatological annual means of H_s and θ_m for the southwest Atlantic Ocean, along the coast of Brazil. Although most of the region shows H_s around 1.75 m, it is possible to observe higher waves coming from the Southern Ocean as well as waves with H_s higher than 2 m in the tropical SAO, approximately between 10° S and 20° S. Additionally, closer to the shore, waves tend to become smaller, mainly in enclosed areas, where there are major river mouths, which is the case for the Amazon River in the north of Brazil and the Rio de La Plata at the border between Argentina and Uruguay.

The distribution of the climatological annual means of H_s^{wv} and θ_m^{wv} , and H_s^s and θ_m^s , are shown in Figure 4. The differences between the wind sea- and swell-related parameters are easily noticeable. While the mean H_s^s reaches 2.5 m, with most of the offshore region ranging from 1.5 m and 1.75 m, the mean H_s^{wv} does not exceed 1.5 m. Moreover, mean wave directions also differ between the two scenarios, with a larger contribution of SE and NE waves among the swell waves and E waves among the wind sea waves.

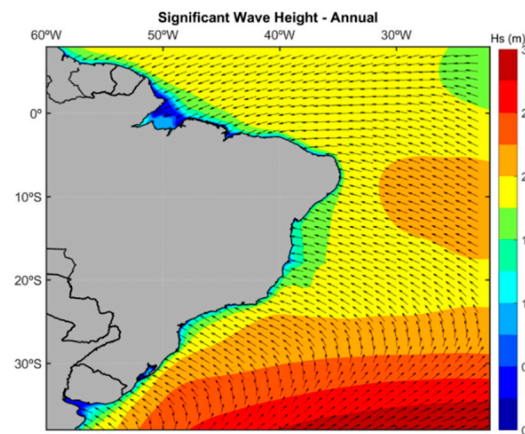


Figure 3. Annual mean H_s (m) and θ_m ($^\circ$), for Brazil.

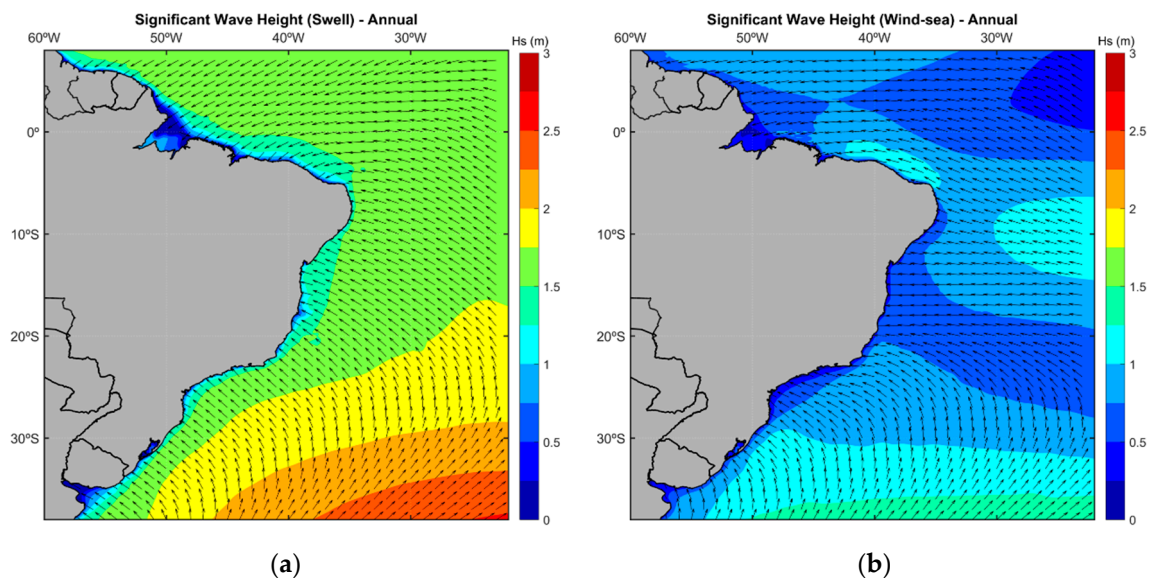


Figure 4. (a) Annual mean H_s^s (m) and θ_m^s ($^\circ$), for Brazil. (b) Annual mean H_s^w (m) and θ_m^w ($^\circ$), for Brazil.

By dividing the climatological means of H_s^w by H_s^s , it is possible to observe the prevalence of wind sea or swell in the study area (Figure 5). Except for the north region of Brazil and the coast of Bahia along the eastern coast, the results indicate a swell predominance over wind sea waves, with values lower than 1. Moreover, the predominance of wind sea waves at the major river mouths is even clearer than in the annual H_s results shown previously. Furthermore, the effect of the wind jets along the northern coast of Brazil is also more visible, with wind sea waves being almost as relevant as swell waves, which is represented by values around 1, indicating equal importance from both components. Areas closer to the coast indicate even higher values, representative of wind sea-dominated regions.

3.3. Extreme Wave Events

Extreme storm waves are characterized by uncommonly high wave heights. The extreme H_s values were calculated as the 95th percentile (P95) [44]. Showing the climatological P95 results for the study area, Figure 6a reveals a latitudinal variation for most of the study area, from around 2 m in the tropical latitudes to more than 5 m in the subtropical SAO. Across the offshore area of Brazil, values between 2 m and 3.5 m are visible. However, the regions closer to the coast show values up to 2.5 m only. Accordingly, the maximum H_s shown in Figure 6b also exhibits a decrease from the south of Brazil towards lower latitudes, with the lowest values in the equatorial region and the highest ones across the

extra-tropical latitudes. Values above 10 m can only be found below 25° S and the entire north region of Brazil presents a maximum H_s lower than 4 m, while the southeastern and eastern regions show values ranging from 4 m to 7 m.

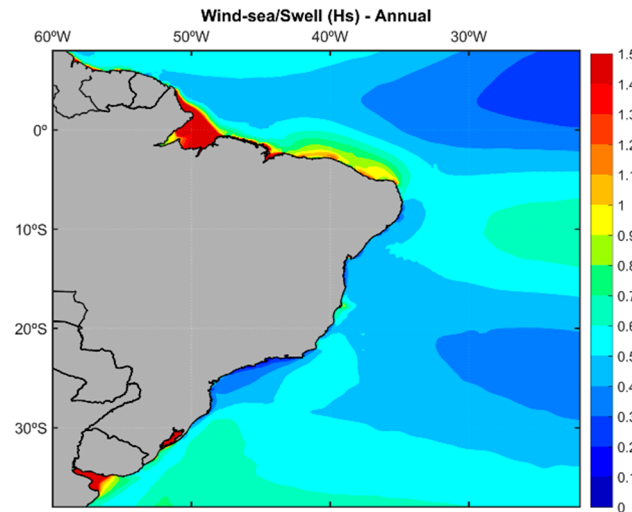


Figure 5. Annual mean swell prevalence based on H_s (dimensionless) for Brazil.

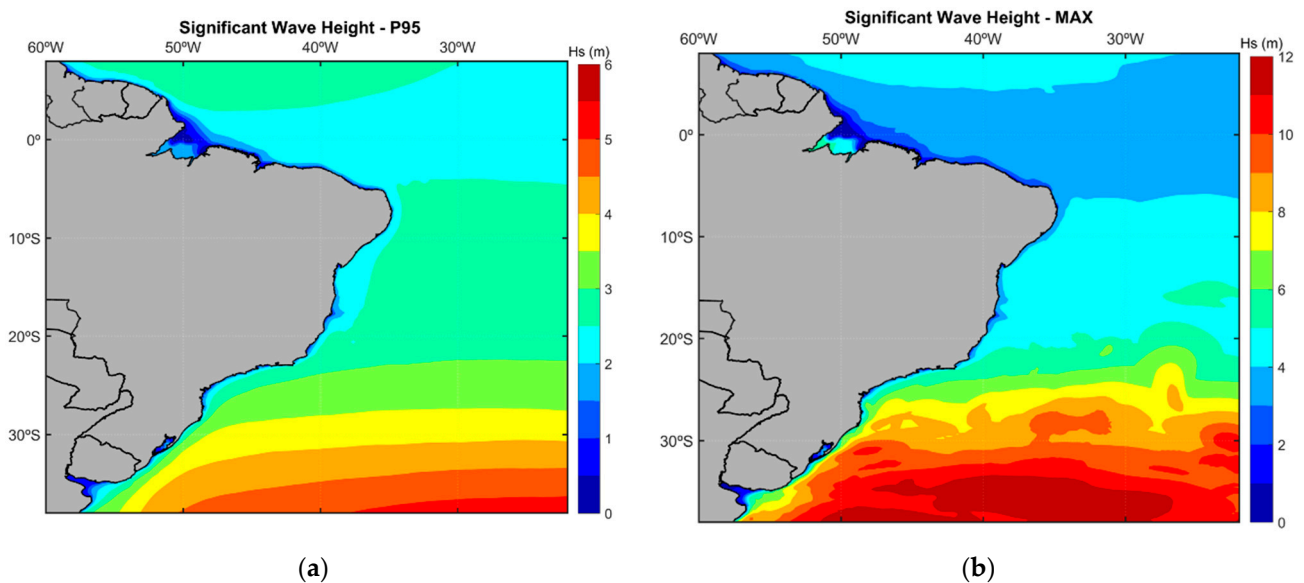


Figure 6. (a) Annual 95th percentile of H_s (m) for Brazil. (b) Annual maximum H_s (m) for Brazil.

In general, the extreme H_s values in the study area are relatively low when compared to other regions of the world, such as the North Atlantic and North Pacific Oceans. Even higher latitudes of the SAO present higher extreme H_s values than the Brazilian coast [45].

3.4. Wave Energy Flux

The wave energy flux (or the ability of the waves to perform work, in $\text{kw}\cdot\text{m}^{-1}$) is defined here as P_w . The wave energy flux is a function of the wave periods and wave heights, to the first and second order, respectively [4]. Figure 7a displays the climatological annual means of P_w for the coast of Brazil. Overall, with the exception of the extratropical region, P_w is relatively low across the study area. However, higher values of wave power can be observed across the area where the most extreme waves were found. These waves most likely represent the edges of the Southern Ocean storm generation area.

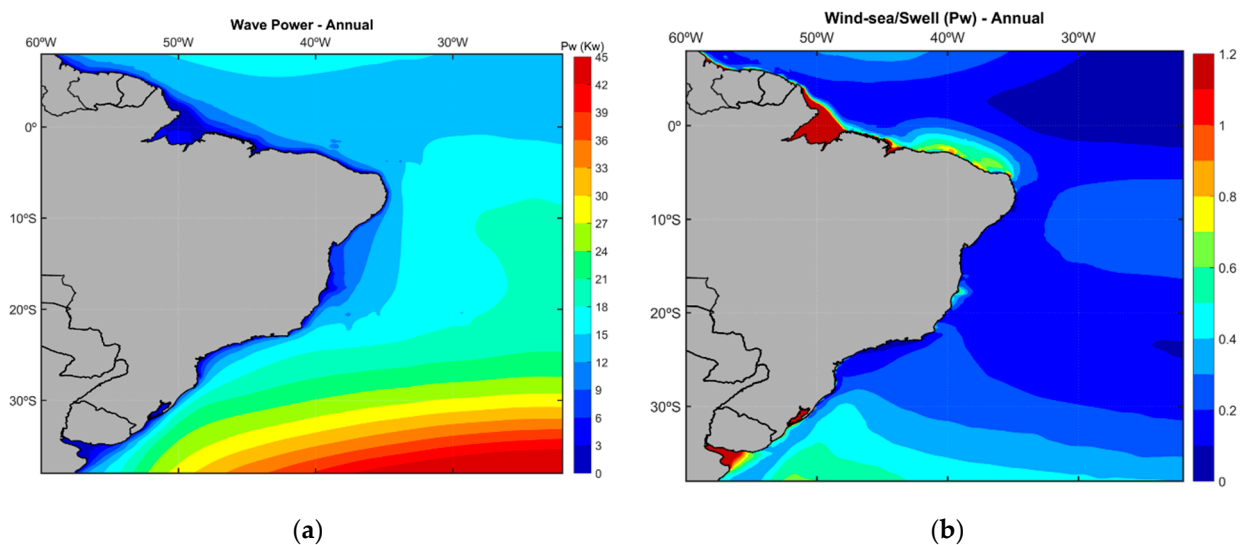


Figure 7. (a) Annual mean P_w (kw) for Brazil. (b) Annual distribution of swell prevalence based on P_w (dimensionless) for Brazil.

Figure 7b shows the distribution of swell prevalence based on wave power by comparing P_w^w and P_w^s . The low values indicated in Figure 7b represent a higher predominance of P_w^s than P_w^w . This is a consequence of the fact that swell waves carry most of the ocean energy and are more regular than wind sea waves.

Additionally, the P_w geographical distribution (Figure 7a) is similar to that of P95 (Figure 6a), with the lowest values closer to the shore and along the equatorial region and the highest values across the extra-tropical region. The influence of the coastal low-level wind jets along the north coast of Brazil can, once again, be observed when comparing the relationship between P_w^w and P_w^s (Figure 7b), with the local wind generating higher wind sea wave heights, closer to H_s^s .

3.5. Swell Events

Due to their dispersive properties, waves propagate freely away from their generation areas. Given similar conditions some waves might have as a result of the same generation storm, the waves tend to group themselves, constructing a swell event. These swell events can then be identified depending on the behavior of the peak wave period and peak mean wave direction. In order to isolate such events from the remaining local sea-state conditions, a swell-tracking algorithm was applied to 50 points along the coast of Brazil [40–42].

After choosing approximately equally distanced points along the coast of Brazil, the swell identification algorithm identified all individual swell events (from ERA-5H) that occurred at each of the coastal positions. Figure 8 displays the climatological annual mean number of swell events at each location, with a minimum of 0 events and a maximum of 12 events per year. Note that these values correspond to specific (pure) swell events that fill the criteria used in the algorithm. It is possible to observe that almost the entire north region of Brazil has an annual average of less than six swell events per year. On the other hand, the south and southeast regions range between 0.1 and 9 events, and the highest values are found along the east and northeast regions.

As mentioned, besides identifying and counting the swell events at each location, the swell-tracking algorithm can also estimate the approximate origin location and time of such events. Table A1 in Appendix A displays the results and coordinates for all 50 points selected for this analysis. To exemplify the results, 6 points were chosen from the original 50 points, and their results are presented in Table 3, which displays the contribution of multiple generation areas to the percentage of swell events coming from each section of the Atlantic Ocean basin. The southern points (4 and 11; Figure 8) indicate the SAO as being responsible for most of the swell events arriving in the region, while over 80% of the swell

events arriving on the points in the northeast and north regions (31, 37, and 45) originate in the NATL. In addition, even though almost 72% of the events arriving at the eastern region (point 22) originated from storms in the SAO, over 10% originated in the Tropical Atlantic Ocean (TAO), possibly related to tropical cyclone activity.

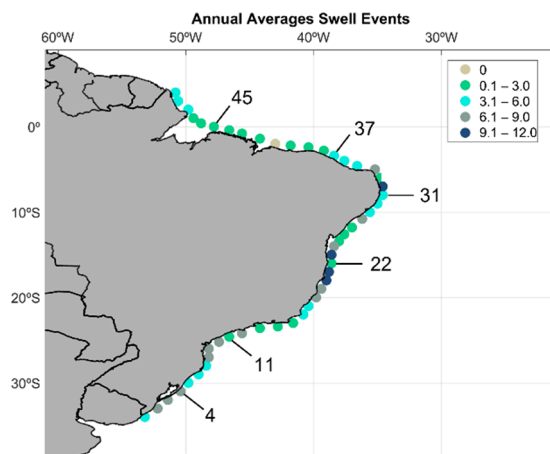


Figure 8. Annual mean number of swell events for Brazil, and the location of the six key points.

Table 3. Percentages of the number of swell events (%) originating in each area of the Atlantic Ocean: North Atlantic Ocean (NATL), Tropical Atlantic Ocean (TAO), and South Atlantic Ocean (SAO).

Point	NATL	TAO	SAO	Atlantic Swells
45	97.6	0.8	0.0	98.4
37	89.4	2.5	0.0	91.9
31	87.9	0.6	0.0	88.5
22	0.0	13.3	71.7	85.0
11	0.0	7.4	86.8	94.1
4	0.0	0.7	89.5	90.2

Furthermore, none of the selected six points have the full 100% of their swell events formed in the Atlantic Ocean (Table 3). For instance, point 22 has the lowest percentage of Atlantic swells with 85%, out of which 13.3% originated in the TAO and 71.7% in the SAO. On the other hand, point 45 displays the highest percentage of Atlantic swell (98.4%), almost entirely originating in the NATL (97.6%). This result indicates that the Brazilian coast receives swell waves from other regions of the global ocean, such as the South Pacific and South Indian oceans.

3.6. Large Scale Atmospheric Forcing

Several studies have shown the possibility of wave climate variability being associated with atmospheric oscillations and modes, usually depicted as climate indices. The relevance of these events on wave climate has been proven by the control NAO has over H_s of the NATL [16,46,47]. The NAO is the principal mode of sea-level pressure (SLP) variability in the NATL. The spatial pattern of the NAO consists of a dipole structure between the Azores' high-pressure system and the Icelandic low-pressure system. During the positive phase of the NAO, the oscillation represented in this mode consists of a strong anticyclone over the Azores, extending its crest along the subtropical latitudes of the NATL and promoting free zonal circulation (storm belt), generally above 40° N. This, in turn, leads to strong westerly winds along the middle latitudes, generating bigger waves [16]. As a result, the wave generation processes in the NATL are influenced and, consequently, so are the swells arriving in Brazil.

Through a positive correlation, the results in Figure 9a show that a positive NAO value would be associated with the increase in H_s along part of the northern coast of Brazil

as a result of higher H_s values in the NATL, propagating southwards as swell. However, most of the H_s values in the study area are negatively correlated with NAO, pointing to a decrease in H_s along the eastern and south-eastern coasts of Brazil during the positive NAO phase. Previous research [16] also concluded this by determining that latitudes off the storm areas, such as most of the study area, are subject to waves that are smaller than normal during the positive phase of NAO due to a narrower directional window of wind and waves.

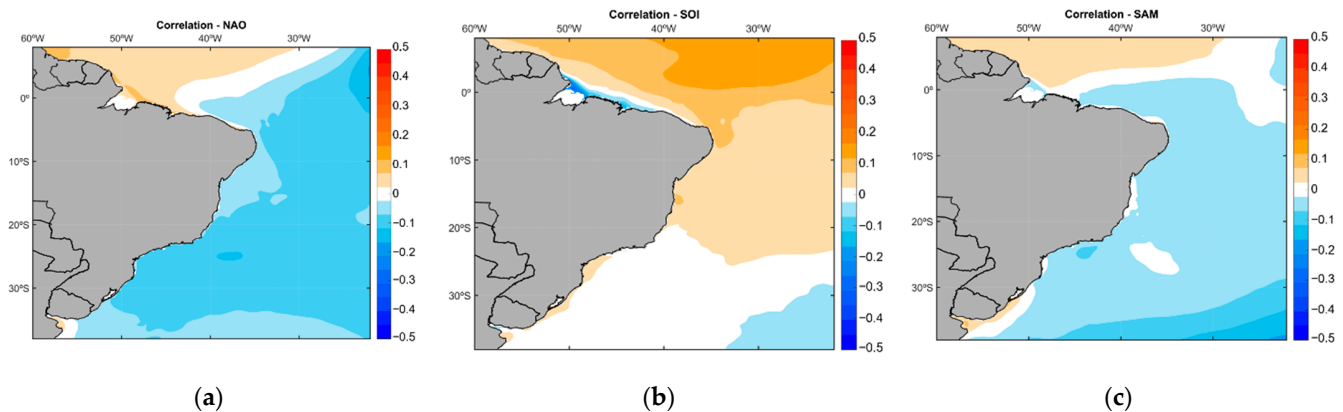


Figure 9. Spatial correlations (dimensionless) of H_s with NAO (a), SOI (b), and SAM (c).

The second climate mode analyzed in this study is the ENSO, which is a global phenomenon with a marked interannual variability. Even though this mode is centered in the equatorial Pacific Ocean, its influence has been proven globally. Moreover, ENSO is indirectly influenced by changes in global temperature and climate change [48]. For instance, previous authors [49] showed that the Atlantic Ocean can affect ENSO by influencing tropical circulation. For example, when the ascending branch of the Walker circulation is strengthened in the Atlantic Ocean, there is an associated stronger descending branch in the Pacific Ocean resulting in ocean surface divergence and, consequently, the development of La Niña.

The most common index to represent ENSO is the SOI. While a positive SOI value is representative of La Niña events, a negative SOI value corresponds to El Niño phases. Most of the Brazilian coast indicates an increase in H_s during positive phases of ENSO, as shown by the positive correlations in Figure 9b. The results here agree with [50], who concluded that, during El Niño years, there is a reduction in H_s of up to 8 cm in the northwest part of the SAO.

However, as the results showed, the offshore region of the south and southeast coasts of Brazil showed no correlation against SOI. This possibly happens because, during the negative SOI phase, there is an intensification of the subtropical jets blocking cold fronts traveling from higher latitudes, leading to a decrease in the incidence of S-SW waves, representative of regional storm waves and swell waves, which typically have a higher H_s values [35,51].

The SAM is the leading variability mode affecting the Southern Hemisphere (SH) atmospheric circulation, responsible for approximately 30% of the climate variability in the region [18,22]. A positive SAM value is associated with weaker westerlies from 30° S to 50° S and stronger westerlies from 50° S to 70° S in the storm belt over the Southern Ocean. This dipole suggests that during positive SAM periods, extreme wave conditions are favored in the higher latitudes of the SH. However, given the compression of the Subantarctic Front during positive SAM periods with the storm belt contracting towards Antarctica [52], even though the associated waves are higher than average, they have to travel further to reach Brazil, thus losing some of their energy and, consequently, decreasing in height, as shown by the negative correlations in Figure 9c.

4. Key Points Analysis

4.1. In Situ vs. ERA-5H Analysis

The results of the evaluation of ERA-5H performance compared to in situ observations (H_s), are illustrated in Figure 10. The scatterplots compare the in situ measurements with selected key points from the ERA-5H H_s . The buoys and their respective key points have similar coordinates. The ERA-5H grid points were chosen as the closest ones to the actual location of the corresponding buoys they were intended to be compared to. In addition to the scatter plots, linear regression fits were computed, as well as the bias, *RMSE*, correlation coefficient (r), and *SI*. All statistics are overlaid on the scatter plots.

The correlation coefficients show an acceptable relationship between the modeled and observed H_s , with values above 0.70 for all locations, with the highest correlations in Santos and Rio Grande (0.93 and 0.91, respectively) and the lowest in Porto Seguro (0.70). Overall, ERA-5H shows a slight overestimation of H_s in Fortaleza, Recife, and Porto Seguro, but it underestimates H_s in Santos and Rio Grande.

All locations showed *RMSE* values below 0.4, indicating that ERA-5H can represent the observed H_s climate with reasonable accuracy. Moreover, although all five cases show similar scatter indexes, the *SI* results indicate that ERA-5H has the most similar H_s to the Fortaleza buoy (12.64%) and that it differs the most from the waves recorded in Porto Seguro (24.61%).

4.2. Intra-Annual Variability

Figure 11 displays the intra-annual variability (monthly averages) of U_{10} , H_s , H_s^w and H_s^w , and T_m , T_m^w and T_m^w , at the five key points selected for the buoy analysis.

The results show latitudinal variation with stronger seasonality in the equatorial region. Most of the variables follow the same pattern with higher values during the austral winter when the most powerful waves occur, propagated from the extratropical SAO. However, P1 stands out for the opposite seasonality signals when comparing wind sea and swell conditions, with the former always following the wind behavior. Regarding H_s , while all points show higher values of H_s^s than H_s^w for every month, P1 displays the opposite from July to October, coinciding with the period of stronger winds as well. Furthermore, unlike the other locations, in P1, it is noticeable that some of the variables show their highest values from November to March (Figure 11a).

The different seasonality shown at P1 could be associated with the fact that the wave climate in the north region of Brazil responds directly to the ITCZ behavior and is highly influenced by atmospheric and marine climates of the Northern Hemisphere (NH). As the ITCZ moves southward in the austral summer, waves from the NH can reach the north coast of Brazil as a result of the northeasterly trade winds and more intense storm activity creating swell events [53].

The southern points (P4 and P5, Figure 11d,e) are under the influence of polar front systems and seasonal oscillations of the intensity and position of the St. Helena High. The same can be concluded in the central points (P2 and P3, Figure 11b,c) but to a lower extent [54]. Additionally, cold fronts in Brazil are more frequent during the austral winter, as described by [38], which could explain the most energetic waves during this period in the southern region. In contrast, in the northern region, the extreme wave conditions are mostly driven by the NH's circumstances [54,55].

Moreover, intra-annual variability of the wave climate off the coast of Brazil can be analyzed through seasonal spatial distributions of H_s and T_m as well as monthly anomalies of H_s , all of which can be found in the Supplementary Material.

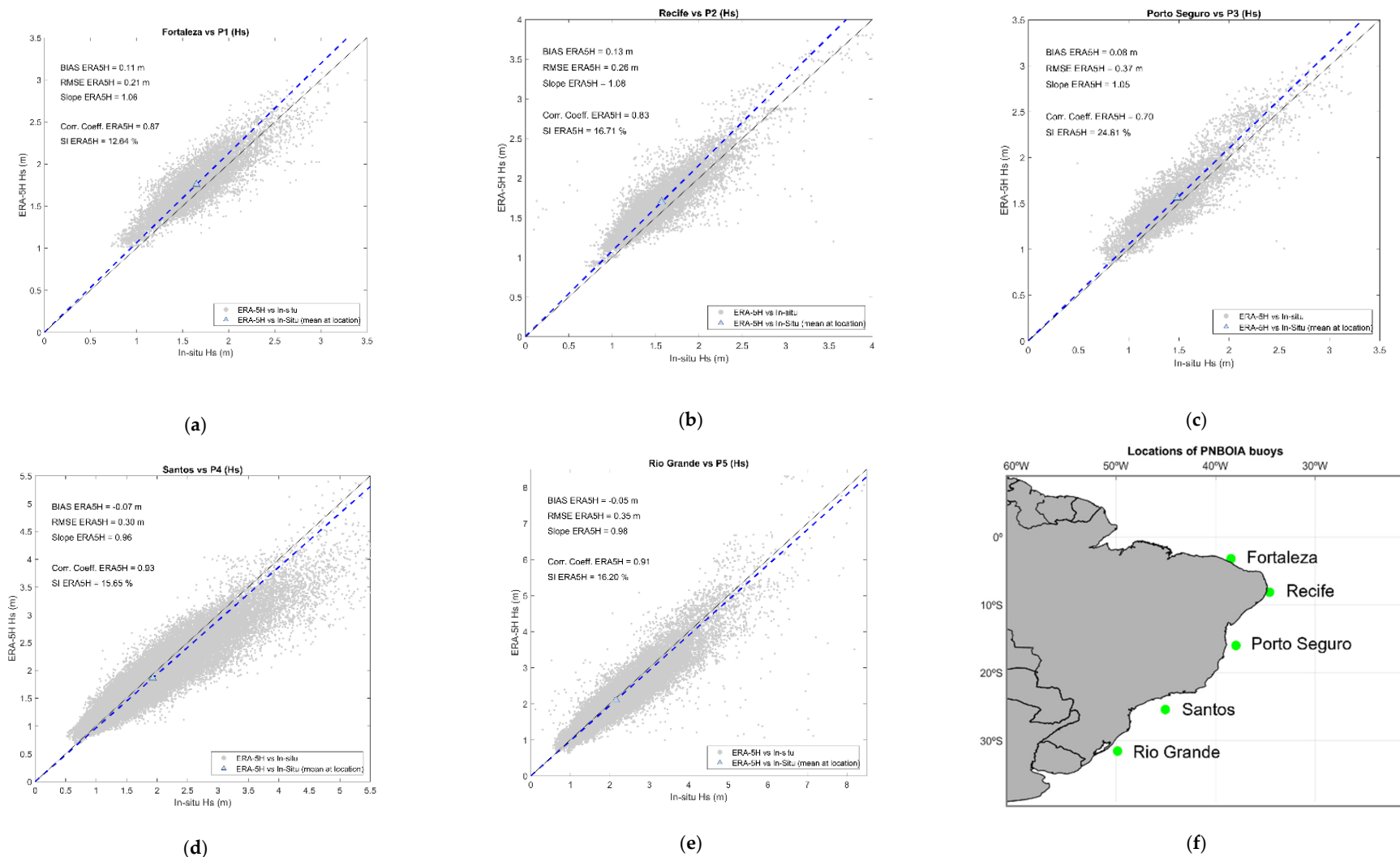


Figure 10. Scatterplot of in situ H_s observations (m) vs. ERA-5H H_s (m) for Fortaleza vs. P1 (a), Recife vs. P2 (b), Porto Seguro vs. P3 (c), Santos vs. P4 (d), and Rio Grande vs. P5 (e) with the respective statistics (BIAS, RMSE, slope, correlation coefficient, and SI) between observed H_s and their respective ERA-5H key points. The blue dashed line represents the linear regression fit. (f) Locations of the buoys.

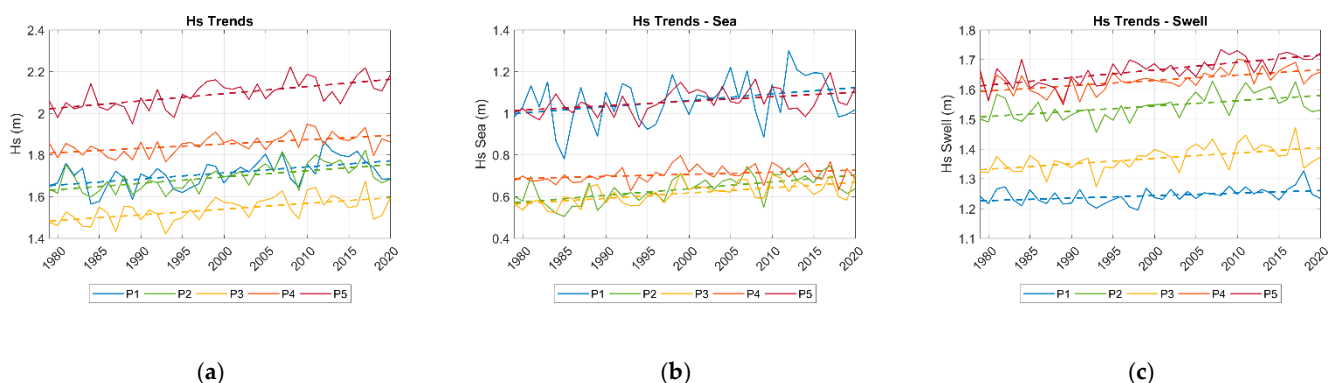


Figure 12. Yearly means and trends for H_s (a), H_s^w (b), and H_s^s (c), for each key point selected within the ERA-5H dataset.

Table 4. Yearly mean H_s trends ($\text{cm}\cdot\text{dec}^{-1}$), H_s^w trends ($\text{cm}\cdot\text{dec}^{-1}$), and H_s^s trends ($\text{cm}\cdot\text{dec}^{-1}$) for each key point selected within the ERA-5H dataset. Significant results for 95% confidence interval are underlined and for 99% are in bold.

Key Points	H_s Rates ($\text{cm}\cdot\text{dec}^{-1}$)	H_s^w Rates ($\text{cm}\cdot\text{dec}^{-1}$)	H_s^s Rates ($\text{cm}\cdot\text{dec}^{-1}$)
P1	2.9	3.0	0.8
P2	3.0	3.2	<u>1.8</u>
P3	2.7	2.5	1.8
P4	<u>2.1</u>	1.0	1.8
P5	3.4	<u>2.1</u>	2.5

Regarding H_s and H_s^s , P5 presented the highest rates ($3.4 \text{ cm}\cdot\text{dec}^{-1}$ and $2.5 \text{ cm}\cdot\text{dec}^{-1}$, respectively). On the other hand, for H_s^w , P2 showed the highest rate ($3.2 \text{ cm}\cdot\text{dec}^{-1}$). P4 presented the lowest rates for all three parameters analyzed.

Most of the Brazilian coast presented a higher rate for H_s^w than for H_s^s , except for P4 and P5 located in the southeast and south regions, respectively. This indicates a possible increase in the local wind over the central and northern points of the coast. The importance of local wind and wind sea waves along the northern coast has been pointed out previously in this study. Furthermore, the positive trend of H_s^s along the southern regions could be an indication of increased wind speed in the storm generation areas of the SAO.

Regarding the positive trends in the northern and central sectors, these could be associated with an increase in storm activity in the NH [56]. In contrast, the increase in H_s along the southern regions may have been associated with the SAM positive trend since the 1960s [18,57], although the present study indicated a negative correlation between H_s and SAM in this region. However, because the present correlation analysis did not isolate swell waves or winter conditions, the possible influence of the SAM positive trend could have been masked by wind sea waves and summer conditions.

The increase in H_s over the last four decades, observed in the present study, was also noted in the NATL [16,28], and a shift from a negative to a positive H_s trend in the 1990s was detected in Italy [27]. Several hypotheses have been raised to explain it, such as interannual and inter-decadal variabilities, long-term trends driven by global climate change, storm activities, and greenhouse gas concentrations [29]. Moreover, several studies have discussed the possibility of the upward trend from the mid-1960s and 1970s being associated with the improvement of aerial observations and the beginning of the satellite era around the same period. This would be due to the fact that, as a result, the development of both the monitoring and understanding of wind and atmospheric pressure occurred, essential for wave studies in general [24,58].

Furthermore, an increase in sea surface temperature (SST) as a result of climate change may be leading to an increase in wave energy, implying an increase in either wave height or period, or even both. By statistically comparing global wave energy flux and SST, previous

authors [59] found a significant positive correlation between the two, as well as a positive trend of the former of 0.4% per year since 1948. The authors based their conclusion on the fact that wind waves respond to the wind regime, which, in turn, is critically influenced by SST.

5. Conclusions

A qualitative analysis of the wave climate off the coast of Brazil, from the high-resolution ECMWF global hindcast ERA-5H, has been presented here. The higher temporal and geographical resolutions of ERA-5H, when compared to other wave hindcasts and reanalyses, allowed a better representation and understanding of the wave climate of the SAO.

The analysis was performed for wind sea and swell waves separately, as well as for the total sea-state wave conditions. It has been shown that the wind sea and swell characteristics in the SAO agree with the global knowledge that swell waves are higher, more energetic, and more prevalent in the open ocean than wind sea waves [4,43,60].

Extreme wave events and wave energy content were examined through extreme wave heights (P95), maximum wave heights, and wave power (wave energy flux). All three variables presented a similar geographical distribution, with the lowest values closer to the shore and along the equatorial region and the highest ones across the extra-tropical region, which most likely represent the edges of the Southern Ocean storm generation area.

Because of the propagation effect of the waves, changes in H_s are most likely related to changes in the conditions of the storm generation areas rather than a direct response to changes in regional wind speed. Thus, an examination of the swell events arriving at the coast of Brazil was performed to better understand where such waves are coming from. The results showed that even though the study area is sheltered from the Indian and Pacific Oceans, not all swell events originate in the Atlantic Ocean. For instance, as we move towards the central region of Brazil, the contribution of Atlantic swells decreases to approximately 75%, as opposed to the 85% of Atlantic swells detected in the northern and southern regions. These results indicate that the Indian and Pacific Oceans also have a relevant contribution and should be considered in studies involving the impact of climate forcing and climate change over the wave climate of the SAO.

Still, given the high contribution of the Atlantic Ocean in the study area, the influence of large-scale atmospheric circulation patterns on the H_s climate was investigated through correlations with the NAO, SOI, and SAM indices. Although at different levels, both the NAO and the SAM were shown to have a negative correlation with most of the study area, apart from the most northern region. Yet, the values were all very low. On the other hand, SOI was shown to have relatively higher positive correlation values across the entire offshore tropical area and the northern region of the coast. It also showed a positive correlation with the central region, although at a lower level.

It should be pointed out that similar studies compute this correlation by separating winter and summer conditions [50]. However, in the present study, the entire time series was considered, which could lead to inaccurate results since certain climate modes peak at different periods of the year.

The ERA-5H H_s data were also compared against in situ data from five different buoys along the coast of Brazil. The results showed an underestimation of H_s along the southern regions of the study area, where the correlation coefficients were also the highest between observed and modelled data.

Past studies have outlined such behavior regarding ERA-5. For instance, previous research [61] detected an underestimation (overestimation) of H_s in swell-dominated areas (wind sea-dominated areas). Here, ERA-5H seems to be moving in the same direction, underestimating H_s in the southernmost locations. These areas were also described as swell-dominated regions in the present study. On the other hand, an overestimation of H_s along the northern coast of Brazil has been shown. This area has been described here as a wind-sea-dominated region.

The long-term variability of the significant wind sea and swell wave heights was investigated separately to assess how they combine to influence the long-term trends of the H_s in the SAO. The upward trend of H_s observed here could be a result of the intensification of the westerlies along the SH projected for the 21st century as described by [62]. According to the authors, this mechanism would lead to an increase in the climatological extreme wave heights, such as maximum H_s , as a result of the poleward shift of extratropical storms. This process is also represented by the significant trend toward the positive phase of SAM since the mid-1960s [18,57]. Another supporting result for such an assumption is the latitudinal variation of the H_s^s trends shown in the present study, with the highest rates at higher latitudes.

For a clearer view of the wave conditions in the area and how these might change under a climate change scenario, further studies are needed, involving the inter-relationships of different climate modes as well as different storm generation areas.

Supplementary Materials: The following supporting information can be downloaded at: <https://www.mdpi.com/article/10.3390/cli10040053/s1>, Figure S1: Spatial distribution of annual averages of H_s (m) (a), P95 (m) (c), P_w (Kw) (e) and P95 of P_w (Kw) (g) based on ERA5, for Brazil. Spatial distribution of annual averages of H_s (m) (b), P95 (m) (d), P_w (Kw) (f) and P95 of P_w (Kw) (h) based on ERA-5H, for Brazil; Figure S2: Spatial distribution of seasonal averages of H_s (m) and θ_m (°) for (a) DJF, (b) MAM, (c) JJA, and (d) SON, for Brazil; Figure S3: Spatial distribution of seasonal averages of T_m (s) and θ_m (°) for (a) DJF, (b) MAM, (c) JJA, and (d) SON for Brazil; Figure S4: Spatial distribution of H_s anomalies (m) per month for Brazil.

Author Contributions: Conceptualization, A.S.; methodology, A.S. and G.L.; software, C.S.C. and G.L.; formal analysis, C.S.C.; investigation, C.S.C.; data curation, G.L.; writing—original draft preparation, C.S.C.; writing—review and editing, C.S.C., A.S. and G.L.; visualization, C.S.C.; supervision, A.S. All authors have read and agreed to the published version of the manuscript.

Funding: Gil Lemos acknowledges funding from Fundação para a Ciência e a Tecnologia (FCT), Grant FCT—UIDB/50019/2020—IDL.

Data Availability Statement: ERA-5 data can be downloaded from this website: <https://cds.climate.copernicus.eu/cdsapp#!/dataset/reanalysis-era5-pressure-levels?tab=overview> (accessed on 22 March 2021). ERA5-H is a new hindcast dataset under production; data are available on reasonable request. Observational (in situ) buoy data can be downloaded from this website: <https://www.marinha.mil.br/chm/dados-do-goos-brasil/pnboia-mapa> (accessed on 8 June 2021).

Conflicts of Interest: The authors declare no conflict of interest.

Appendix A

In this appendix, the results of the swell-tracking algorithm analysis for the entire coast of Brazil are displayed.

Table A1. Coordinates of the points used in the swell-event analysis and their respective annual mean number of swell events, total number of swell events, and percentages of swells (%) coming from each storm-originating area in the Atlantic Ocean: North Atlantic Ocean (NATL), Tropical Atlantic Ocean (TAO), and South Atlantic Ocean (SAO).

Points	Coordinates		Swell Events		Swell Origin Areas (%)			
	Latitude	Longitude	Yearly Average	Total	NATL	TAO	SAO	Atlantic Ocean
1	−34	−53.2	5.4	226	0.0	0.9	81.9	82.7
2	−33	−52.2	7.0	294	0.0	0.7	84.4	85.0
3	−32	−51.4	7.1	299	0.0	0.7	89.0	89.6
4	−31	−50.4	7.3	306	0.0	0.7	89.5	90.2

Table A1. Cont.

Points	Coordinates		Swell Events		Swell Origin Areas (%)			
	Latitude	Longitude	Yearly Average	Total	NATL	TAO	SAO	Atlantic Ocean
5	−30	−49.8	5.7	238	0.0	0.4	88.2	88.7
6	−29	−49	5.0	210	0.0	1.0	85.2	86.2
7	−28	−48.4	5.4	228	0.0	5.3	81.6	86.8
8	−27	−48.2	6.3	265	0.0	6.8	78.5	85.3
9	−26	−48.2	7.4	311	0.0	3.9	83.9	87.8
10	−25.2	−47.4	7.2	304	0.0	4.3	79.9	84.2
11	−24.6	−46.6	2.8	116	0.0	7.4	86.8	94.1
12	−24.2	−45.6	8.5	356	0.0	6.2	79.2	85.4
13	−23.6	−44.2	1.5	62	0.0	25.8	45.2	71.0
14	−23.4	−42.8	1.9	81	0.0	17.3	50.6	67.9
15	−23	−41.6	2.3	96	0.0	19.8	54.2	74.0
16	−22	−40.8	3.1	129	0.0	10.1	59.7	69.8
17	−21	−40.4	4.8	200	0.0	6.0	73.0	79.0
18	−20	−39.8	7.0	294	0.0	4.1	68.0	72.1
19	−19	−39.4	8.0	338	0.0	2.7	68.0	70.7
20	−18	−39	10.7	448	0.0	0.4	69.2	69.6
21	−17	−38.8	11.9	501	0.0	0.6	66.7	67.3
22	−16	−38.6	1.4	60	0.0	13.3	71.7	85.0
23	−15	−38.6	10.0	418	0.0	3.3	61.5	64.8
24	−14	−38.4	6.8	285	0.0	13.0	52.6	65.6
25	−13.4	−38	1.7	71	0.0	12.7	43.7	56.3
26	−12.6	−37.6	0.6	26	15.4	7.7	19.2	42.3
27	−11.8	−37	1.5	64	71.9	10.9	0.0	82.8
28	−10.8	−36.2	6.3	264	85.2	0.8	0.0	86.0
29	−10	−35.6	3.6	152	88.8	0.0	0.0	88.8
30	−9	−35	3.2	135	90.4	0.0	0.0	90.4
31	−8	−34.6	4.1	174	87.9	0.6	0.0	88.5
32	−7	−34.6	9.5	399	82.5	0.5	0.0	83.0
33	−6	−34.8	1.9	78	0.0	6.4	76.9	83.3
34	−5	−35.2	8.8	371	86.5	0.0	0.0	86.5
35	−4.6	−36.6	5.9	246	87.8	0.8	0.0	88.6
36	−4	−37.6	3.4	142	92.3	0.7	0.0	93.0
37	−3.4	−38.4	3.8	161	89.4	2.5	0.0	91.9
38	−2.8	−39.2	2.9	121	96.7	1.7	0.0	98.3
39	−2.4	−40.4	2.4	100	97.0	2.0	0.0	99.0
40	−2.2	−41.8	0.2	7	100.0	0.0	0.0	100.0
41	−2	−43	0.0	0	0.0	0.0	0.0	0.0
42	−1.4	−44.2	2.2	91	86.8	0.0	0.0	86.8
43	−0.8	−45.6	2.1	90	98.9	0.0	0.0	98.9

Table A1. Cont.

Points	Coordinates		Swell Events		Swell Origin Areas (%)			
	Latitude	Longitude	Yearly Average	Total	NATL	TAO	SAO	Atlantic Ocean
44	−0.4	−46.6	2.6	110	0.0	5.5	83.6	89.1
45	0	−47.8	3.0	126	97.6	0.8	0.0	98.4
46	0.4	−48.8	2.8	119	0.0	5.9	76.5	82.4
47	1	−49.4	3.0	124	0.0	3.2	80.6	83.9
48	2	−49.8	3.9	164	0.0	4.9	80.5	85.4
49	3	−50.6	3.7	157	0.0	5.7	80.3	86.0
50	4	−50.8	4.5	191	0.0	2.6	74.3	77.0

References

- Cuchiara, D.C.; Fernandes, E.H.; Strauch, J.C.; Calliari, L.J. Modelagem Numérica do Comportamento das Ondas na Costa do Rio Grande do Sul. In Proceedings of the II Seminário e Workshop em Engenharia Oceânica, Rio Grande, Brazil, 23–25 November 2006.
- Sempreviva, A.M.; Schiano, M.E.; Pensieri, S.; Semedo, A.; Tomé, R.; Bozzano, R.; Borghini, M.; Grasso, F.; Soerensen, L.L.; Teixeira, J.; et al. Observed development of the vertical structure of the marine boundary layer during the LASIE experiment in the Ligurian Sea. *Ann. Geophys.* **2010**, *28*, 17–25. [[CrossRef](#)]
- Stewart, R.H. *Introduction to Physical Oceanography*; Department of Oceanography, Texas A&M University: College Station, TX, USA, 2005; p. 353. [[CrossRef](#)]
- Semedo, A.; Suselj, K.; Rutgersson, A.; Sterl, A. A Global View on the Wind Sea and Swell Climate and Variability from ERA-40. *J. Clim.* **2011**, *24*, 1461–1479. [[CrossRef](#)]
- Rutgersson, A.; Sætra, Ø.; Semedo, A.; Carlsson, B.; Kumar, R. Impact of surface waves in a Regional Climate Model. *Meteorol. Z.* **2010**, *19*, 247–257. [[CrossRef](#)]
- Holthuijsen, L.H. *Waves in Oceanic and Coastal Waters*; Cambridge University Press: New York, NY, USA, 2007; p. 405.
- Carrasco, A.; Semedo, A.; Isachsen, P.E.; Christensen, K.H.; Sætra, Ø. Global surface wave drift climate from ERA-40: The contributions from wind-sea and swell. *Ocean Dyn.* **2014**, *64*, 1815–1829. [[CrossRef](#)]
- Hughes, S.A.; Miller, H.C. Transformation of Significant Wave Heights. *J. Waterw. Port Coast. Ocean. Eng.* **1987**, *113*, 588–605. [[CrossRef](#)]
- Semedo, A. Seasonal Variability of Wind Sea and Swell Waves Climate along the Canary Current: The Local Wind Effect. *J. Mar. Sci. Eng.* **2018**, *6*, 28. [[CrossRef](#)]
- Pecher, A.; Kofoed, J.P. *Handbook of Ocean Wave Energy*; Springer Open: Aalborg, Denmark, 2017; p. 305.
- Cavaleri, L.; Fox-Kemper, B.; Hemer, M. Wind Waves in the Coupled Climate System. *Bull. Am. Meteorol. Soc.* **2012**, *93*, 1651–1661. [[CrossRef](#)]
- WMO. *World Meteorological Organization. Guide to Wave Analysis and Forecasting*, 2nd ed.; World Meteorological Organization WMO: Geneva, Switzerland, 1998; p. 168.
- Masselink, G.; Gehrels, R. *Coastal Environments & Global Change*; American Geophysical Union and John Wiley & Sons, Ltd: New York, NY, USA, 2014; pp. 299–335. Available online: www.wiley.com/go/masselink/coastal (accessed on 23 December 2019).
- Young, I.R. Seasonal variability of the global ocean wind and wave climate. *Int. J. Climatol.* **1999**, *19*, 931–950. [[CrossRef](#)]
- Marcos, M.; Rohmer, J.; Vousdoukas, M.I.; Mentaschi, L.; Le Cozannet, G.; Amores, A. Increased Extreme Coastal Water Levels Due to the Combined Action of Storm Surges and Wind Waves. *Geophys. Res. Lett.* **2019**, *46*, 4356–4364. [[CrossRef](#)]
- Dodet, G.; Bertin, X.; Taborda, R. Wave climate variability in the North-East Atlantic Ocean over the last six decades. *Ocean Model.* **2010**, *31*, 120–131. [[CrossRef](#)]
- Kumar, P.; Min, S.K.; Weller, E.; Lee, H.; Wang, X.L. Influence of climate variability on extreme ocean surface wave heights assessed from ERA-interim and ERA-20C. *J. Clim.* **2016**, *29*, 4031–4046. [[CrossRef](#)]
- Marshall, A.G.; Hemer, M.A.; Hendon, H.H.; McInnes, K.L. Southern annular mode impacts on global ocean surface waves. *Ocean Model.* **2018**, *129*, 58–74. [[CrossRef](#)]
- Lemos, G.; Semedo, A.; Dobrynin, M.; Behrens, A.; Staneva, J.; Bidlot, J.-R.; Miranda, P. Mid-twenty-first century global wave climate projections: Results from a dynamic CMIP5 based ensemble. *Glob. Planet. Chang.* **2019**, *172*, 69–87. [[CrossRef](#)]
- Menéndez, M.; Mendez, F.; Losada, I.; Graham, N.E. Variability of extreme wave heights in the northeast Pacific Ocean based on buoy measurements. *Geophys. Res. Lett.* **2008**, *35*. [[CrossRef](#)]
- Semedo, A.; Vettor, R.; Breivik, Ø.; Sterl, A.; Reistad, M.; Soares, C.G.; A Lima, D.C. The wind sea and swell waves climate in the Nordic seas. *Ocean Dyn.* **2014**, *65*, 223–240. [[CrossRef](#)]

22. Hemer, M.A.; Church, J.A.; Hunter, J.R. Variability and trends in the directional wave climate of the Southern Hemisphere. *Int. J. Clim.* **2010**, *30*, 475–491. [[CrossRef](#)]
23. Buizza, R.; Brönnimann, S.; Haimberger, L.; Laloyaux, P.; Martin, M.J.; Fuentes, M.; Alonso-Balmaseda, M.; Becker, A.; Blaschek, M.; Dahlgren, P.; et al. The EU-FP7 ERA-CLIM2 Project Contribution to Advancing Science and Production of Earth System Climate Reanalyses. *Bull. Am. Meteorol. Soc.* **2018**, *99*, 1003–1014. [[CrossRef](#)]
24. Dee, D.P.; Balmaseda, M.A.; Balsamo, G.; Engelen, R.; Simmons, A.J.; Thépaut, J.-N. Toward a Consistent Reanalysis of the Climate System. *Bull. Am. Meteorol. Soc.* **2014**, *95*, 1235–1248. [[CrossRef](#)]
25. Aarnes, O.J.; Abdalla, S.; Bidlot, J.-R.; Breivik, Ø. Marine Wind and Wave Height Trends at Different ERA-Interim Forecast Ranges. *J. Clim.* **2015**, *28*, 819–837. [[CrossRef](#)]
26. Young, I.R.; Zieger, S.; Babanin, A.V. Global Trends in Wind Speed and Wave Height. *Science* **2011**, *332*, 451–455. [[CrossRef](#)]
27. Martucci, G.; Carniel, S.; Chiggiato, J.; Sclavo, M.; Lionello, P.; Galati, M.B. Statistical trend analysis and extreme distribution of significant wave height from 1958 to 1999—An application to the Italian Seas. *Ocean Sci.* **2010**, *6*, 525–538. [[CrossRef](#)]
28. Wang, X.L.; Feng, Y.; Swail, V.R. North Atlantic wave height trends as reconstructed from the 20th century reanalysis. *Geophys. Res. Lett.* **2012**, *39*, 1–6. [[CrossRef](#)]
29. Bertin, X.; Prouteau, E.; Letetrel, C. A significant increase in wave height in the North Atlantic Ocean over the 20th century. *Glob. Planet. Chang.* **2013**, *106*, 77–83. [[CrossRef](#)]
30. Moura, M.R. Aspectos Climáticos versus Variação Sazonal do Perfil Morfodinâmico das Praias do Litoral Oeste de Aquiraz, Ceará, Brasil. *Rev. Bras. Climatol.* **2012**, *11*, 208–222. [[CrossRef](#)]
31. Araujo, C.E.S.; Franco, D.; Melo, E.; Pimenta, F. Wave Regime Characteristics of the Southern. In Proceedings of the International Conference on Coastal and Port Engineering in Developing Countries, COPEDEC VI, Colombo, Sri Lanka, 16–20 September 2003; Paper No. 097. p. 15.
32. Sprovieri, F.C. Clima de Ondas, Potencial Energético e o Transporte de Sedimentos no Litoral Norte do Rio Grande do Sul. Ph.D. Thesis, Universidade Federal do Rio Grande do Sul, Porto Alegre, Brazil, 2018.
33. Silva, P.G.; Klein, A.H.; Gonzalez, M.; Gutiérrez, O.Q.G.; Espejo, A. Performance assessment of the database downscaled ocean waves (DOW) on Santa Catarina coast, South Brazil. *An. Acad. Bras. Cienc.* **2015**, *87*, 623–634. [[CrossRef](#)]
34. Oliveira, B.A.; Sobral, F.; Fetter, A.; Mendez, F.J. A high-resolution wave hindcast off Santa Catarina (Brazil) for identifying wave climate variability. *Reg. Stud. Mar. Sci.* **2019**, *32*, 100834. [[CrossRef](#)]
35. Pereira, N.E.D.S.; Klumb-Oliveira, L.A. Analysis of the influence of ENSO phenomena on wave climate on the central coastal zone of Rio de Janeiro (Brazil). *J. Integr. Coast. Zone Manag.* **2015**, *15*, 353–370. [[CrossRef](#)]
36. Pianca, C.; Mazzini, P.L.F.; Siegle, E. Brazilian offshore wave climate based on NWW3 reanalysis. *Braz. J. Oceanogr.* **2010**, *58*, 53–70. [[CrossRef](#)]
37. Espindola, R.L.; Araújo, A.M. Wave energy resource of Brazil: An analysis from 35 years of ERA-Interim reanalysis data. *PLoS ONE* **2017**, *12*, e0183501. [[CrossRef](#)] [[PubMed](#)]
38. Dominguez, J.M.L. The Coastal Zone of Brazil: An Overview. *J. Coast. Res.* **2013**, *39*, 16–20.
39. Hersbach, H.; Bell, B.; Berrisford, P.; Hirahara, S.; Horanyi, A.; Muñoz-Sabater, J.; Nicolas, J.; Peubey, C.; Radu, R.; Schepers, D.; et al. The ERA5 global reanalysis. *Q. J. R. Meteorol. Soc.* **2020**, *146*, 1999–2049. [[CrossRef](#)]
40. Portilla, J. Storm-Source-Locating Algorithm Based on the Dispersive Nature of Ocean Swells. *Avances* **2012**, *4*, C22–C36.
41. Amores, A.; Marcos, M. Ocean Swells along the Global Coastlines and Their Climate Projections for the Twenty-First Century. *J. Clim.* **2020**, *33*, 185–199. [[CrossRef](#)]
42. Lemos, G.; Semedo, A.; Hemer, M.; Menendez, M.; A Miranda, P.M. Remote climate change propagation across the oceans—The directional swell signature. *Environ. Res. Lett.* **2021**, *16*, 064080. [[CrossRef](#)]
43. Chen, G.; Chapron, B.; Ezraty, R.; VanDeMark, D. A Global View of Swell and Wind Sea Climate in the Ocean by Satellite Altimeter and Scatterometer. *J. Atmos. Ocean. Technol.* **2002**, *19*, 1849–1859. [[CrossRef](#)]
44. Campos, R.; Alves, J.-H.; Soares, C.G.; Guimaraes, L.; Parente, C.E. Extreme wind-wave modeling and analysis in the south Atlantic ocean. *Ocean Model.* **2018**, *124*, 75–93. [[CrossRef](#)]
45. Barbariol, F.; Bidlot, J.; Cavaleri, L.; Sclavo, M.; Thomson, J.; Benetazzo, A. Maximum wave heights from global model reanalysis. *Prog. Oceanogr.* **2019**, *175*, 139–160. [[CrossRef](#)]
46. Bacon, S.; Carter, D.J.T. A connection between mean wave height and atmospheric pressure gradient in the North Atlantic. *Int. J. Clim.* **1993**, *13*, 423–436. [[CrossRef](#)]
47. Kushnir, Y.; Cardone, V.J.; Greenwood, J.G.; Cane, M.A. The Recent Increase in North Atlantic Wave Heights. *J. Clim.* **1997**, *10*, 2107–2113. [[CrossRef](#)]
48. NOAA, National Oceanic and Atmospheric Administration PSD (ESRL). El Niño Southern Oscillation (ENSO). 2019. Available online: <https://www.esrl.noaa.gov/psd/enso/> (accessed on 22 March 2021).
49. Rodriguez-Fonseca, B.; Polo, I.; García-Serrano, J.; Losada, T.; Mohino, E.; Mechoso, C.R.; Kucharski, F. Are Atlantic Niños enhancing Pacific ENSO events in recent decades? *Geophys. Res. Lett.* **2009**, *36*, 1–6. [[CrossRef](#)]
50. Ramos, M.S.; Farina, L.; Faria, S.H.; Li, C. Relationships between large-scale climate modes and the South Atlantic Ocean wave climate. *Prog. Oceanogr.* **2021**, *197*, 102660. [[CrossRef](#)]
51. Silva, G.A.M.; Ambrizzi, T.; Marengo, J.A. Observational evidences on the modulation of the South American Low Level Jet east of the Andes according the ENSO variability. *Ann. Geophys.* **2009**, *27*, 645–657. [[CrossRef](#)]

52. Limpasuvan, V.; Hartmann, D.L. Wave-maintained annular modes of climate variability. *J. Clim.* **2000**, *13*, 4414–4429. [[CrossRef](#)]
53. Castro, B.; Brandini, F.; Pires-Vanin, A.; Miranda, L. Multidisciplinary oceanographic processes on the Western Atlantic continental shelf between 4 N and 34 S. *Sea* **2006**, *14*, 259–293.
54. Tessler, M.G.; Goya, S.C. Processos Costeiros Condicionantes do Litoral Brasileiro. *Rev. Dep. Geogr.* **2005**, *17*, 11–23. [[CrossRef](#)]
55. Beserra, E.R.; Mendes, A.L.T.; Estefen, S.F.; Parente, C.E. Wave Climate Analysis for a Wave Energy Conversion Application in Brazil. In Proceedings of the International Conference on Offshore Mechanics and Arctic Engineering—OMAE, San Diego, CA, USA, 10–15 June 2007; pp. 897–902. [[CrossRef](#)]
56. Bender, M.A.; Knutson, T.R.; Tuleya, R.E.; Sirutis, J.J.; Vecchi, G.A.; Garner, S.T.; Held, I.M. Modeled Impact of Anthropogenic Warming on the Frequency of Intense Atlantic Hurricanes. *Science* **2010**, *327*, 454–458. [[CrossRef](#)]
57. Marshall, G.J. Trends in the Southern Annular Mode from observations and reanalyses. *J. Clim.* **2003**, *16*, 4134–4143. [[CrossRef](#)]
58. Killick, R.; Eckley, I.A.; Ewans, K.; Jonathan, P. Detection of changes in variance of oceanographic time-series using changepoint analysis. *Ocean Eng.* **2010**, *37*, 1120–1126. [[CrossRef](#)]
59. Reguero, B.G.; Losada, I.J.; Méndez, F.J. A recent increase in global wave power as a consequence of oceanic warming. *Nat. Commun.* **2019**, *10*, 205. [[CrossRef](#)]
60. Jiang, H.; Chen, G. A Global View on the Swell and Wind Sea Climate by the Jason-1 Mission: A Revisit. *J. Atmos. Ocean. Technol.* **2013**, *30*, 1833–1841. [[CrossRef](#)]
61. Bruno, M.F.; Molfetta, M.G.; Totaro, V.; Mossa, M. Performance Assessment of ERA5 Wave Data in a Swell Dominated Region. *J. Mar. Sci. Eng.* **2020**, *8*, 214. [[CrossRef](#)]
62. Semedo, A.; Weisse, R.; Behrens, A.; Sterl, A.; Bengtsson, L.; Günther, H. Projection of Global Wave Climate Change toward the End of the Twenty-First Century. *J. Clim.* **2013**, *26*, 8269–8288. [[CrossRef](#)]